Materials Transactions, Vol. 48, No. 5 (2007) pp. 903 to 908
Special Issue on New Developments and Analysis for Fabrication of Functional Nanostructures

Low-Temperature Atomic Ordering of Oriented $L1_0$-FePtCu Nanoparticles with High Areal-Density Characterized by Transmission Electron Microscopy and Electron Diffraction

Han Wool Ryu[1,2,*], Kazuhisa Sato[2] and Yoshihiko Hirotsu[2]

[1]*Department of Materials Science and Engineering, Graduate School of Engineering, Osaka University, Suita 565-0871, Japan*
[2]*The Institute of Scientific and Industrial Research, Osaka University, Ibaraki 567-0047, Japan*

Oriented and densely dispersed $L1_0$-FePtCu nanoparticles have been directly synthesized by co-evaporation of Fe, Pt and Cu using rf-magnetron sputtering onto NaCl substrate kept at 563–613 K without any post-deposition annealing. Formation of the $L1_0$-type structure in the specimens fabricated as low a substrate temperature as 563 K ($Fe_{40}Pt_{50}Cu_{10}$) was confirmed by electron microscopy and electron diffraction, while the coercivity measured at room temperature was very low and the intensity of the superlattice reflections was quite weak. The atomic ordering was promoted in the specimen fabricated at 613 K with a composition of $Fe_{37}Pt_{52}Cu_{11}$, resulted in a higher coercivity exceeding 1 kOe at room temperature as well as appearance of clear superlattice reflections. In addition to the evolution of atomic ordering, ⟨100⟩ oriented growth was enhanced as the substrate temperature increased. Particle size dependence of long-range order (LRO) is considered to be responsible for the decrease of coercivity with particle size reduction as well as thermal fluctuation of magnetization. High coercivity was obtained for specimens with Cu concentration near 10 at% under the present sputtering condition. The LRO in the FePtCu ternary phase is considered to sensitively depend on the alloy concentration. [doi:10.2320/matertrans.48.903]

(Received November 8, 2006; Accepted December 21, 2006; Published April 25, 2007)

Keywords: *$L1_0$ structure, transmission electron microscopy, low temperature ordering, sputtering, FePtCu, nanoparticles*

1. Introduction

Since the recent CoCr-based magnetic storage media is confronted with the limit of thermal stability problem,[1)] FePt thin films and nanoparticles with the $L1_0$-type ordered structure have been extensively studied as promising candidates for future ultrahigh density magnetic recording media due to its high magnetocrystalline anisotropy energy (MAE) of 7×10^7 erg/cm^3.[2,3)] Such a high MAE ensures the thermal stability of magnetization of the $L1_0$-FePt nanoparticles, which is suitable for ultra-high density recording higher than 1 Tbit/in^2.[4–6)] Following conditions are required for ultra-high density magnetic storage media: (1) orientation control of magnetic easy axes, (2) high-density dispersion of crystallites with good isolation, and (3) low-temperature synthesis of the $L1_0$ phase. Orientation control as well as isolation of nanoparticles has been achieved by epitaxial growth of FePt alloy onto heated MgO and/or NaCl substrates.[5,7)] However, in order to obtain the $L1_0$ phase with high MAE, it is indispensable to perform the post-deposition annealing or substrate heating at high temperatures around 873 K. Furthermore a few article have taken the areal density of FePt nanoparticles into consideration. Based on such backgrounds, the current interests are concentrated on the fabrication of $L1_0$ FePt nanoparticles with orientation and high-areal density under the lower temperature. Actually, as for the low temperature atomic ordering, several attempts for fabrication of the $L1_0$ phase such as chemical processes,[8,9)] multilayering[10,11)] or ion irradiation[12,13)] have been tried for past years. The most successful method to lower the ordering temperature was addition of the third atomic element like Cu into FePt thin films.[14–16)] However there are a few reports on the Cu addition effect on nanoparticles of FePt alloy. Recently, a formation of FePtCu nanoparticles has been reported by means of chemical routes, but the ordering temperature of 823 K reported is still high.[9)] The present authors have succeeded in fabricating oriented and isolated $L1_0$-type FePtCu nanoparticles under a lower substrate temperature as low as 613 K by means of rf-magnetron sputtering.[17)]

In this study, oriented $L1_0$-type FePtCu ternary islands with high areal density and homogeneous distribution were fabricated by co-deposition of Fe, Pt and Cu targets using rf-magnetron sputtering. Substrate temperature dependence of nanostructure and atomic ordering was studied by transmission electron microscopy and electron diffraction in specific composition. Changes of magnetic properties due to the evolution of atomic ordering were examined from the viewpoints of substrate temperature and alloy composition.

2. Experimental Procedure

Nanoparticles of Fe-Pt-Cu ternary alloy were fabricated by co-deposition of Fe (99.97%), Pt (99.99%) and Cu (99.96%) targets using rf-magnetron sputtering onto NaCl (001) substrate cleaved in air. The sputtering was performed with Ar (99.999%) gas pressure of 1.33 Pa and the power of 30 W with a base pressure of the chamber of 5×10^{-6} Pa. Three kinds of substrate temperatures of 563, 583 and 613 K were used. Post-deposition annealing was not performed after the deposition. Sputtering duration was fixed for 60 s. Thin amorphous carbon film was deposited at room temperature after the sputtering for coating the specimen surface. Structural characterization was performed by using JEOL JEM-2010 and 3000F transmission electron microscopes (TEMs) operated at 200 and 300 kV, respectively. The

*Corresponding author, E-mail: hanryu22@sanken.osaka-u.ac.jp

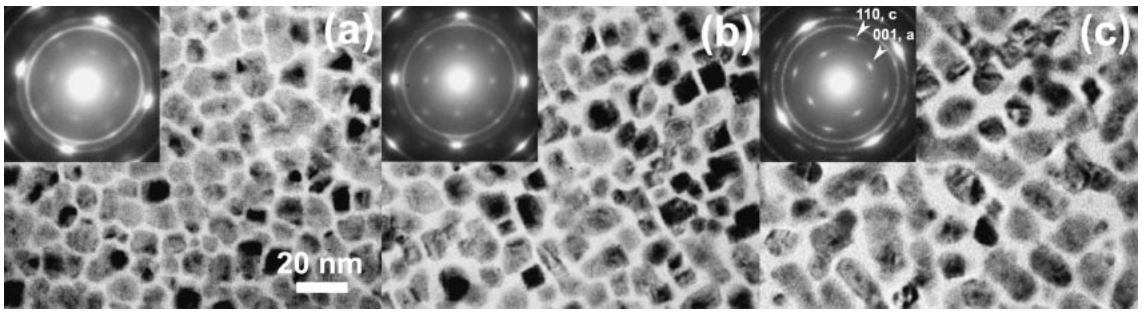

Fig. 1 BF-TEM images and corresponding SAED patterns of FePtCu nanoparticles formed at (a) 563 K, (b) 583 K and (c) 613 K. Indices 110,c and 001,a correspond to crystallographic variants with *c*-axes oriented normal and parallel to the film plane, respectively.

specimen films were mounted on Cu or Mo grids for TEM observation after removing the NaCl substrates in distilled water. TEM images and electron diffraction patterns were digitally recorded on imaging plates (Fuji Film, FDL-UR-V). Alloy compositions were analyzed by energy-dispersive x-ray spectrometer (EDS) attached to 300-kV TEM. Magnetic properties were measured by using a super-conducting quantum interference device magnetometer (Quantum Design MPMS XL) with an applied field up to 50 kOe.

3. Results and Discussion

3.1 Evolution of Atomic Ordering

Proceedings of the atomic ordering reaction toward $L1_0$-ordered phase were studied as a function of the substrate temperature during the sputter-deposition between 563 and 613 K. Bright- field (BF) TEM images and the corresponding SAED patterns for specimens deposited at 563, 583 and 613 K are shown in Figs. 1(a), 1(b) and 1(c), respectively. All the specimens were composed of densely dispersed FePtCu island-like nanoparticles on the substrate surface. According to compositional analyses of individual particles by means of nano-EDS, it was found that compositional difference from one particle to next was quite small. The difference was within their experimental error. All the corresponding SAED patterns include diffraction patterns from the $L1_0$-type ordered structure with ⟨100⟩ orientation grown on the substrate. That is, co-sputtering of Fe, Pt and Cu onto heated NaCl (001) substrate resulted in a direct formation of the $L1_0$-ordered nanoparticles under as low a substrate temperature as 563 K. There exist crystallographic variants in the formation of present FePtCu nanoparticles on the substrate as confirmed by coexistence of 001 and 110 superlattice reflections in the SAED patterns. That is, 001 and 110 reflections correspond to the variants with *c*-axes oriented parallel and normal to the film plane, respectively. Besides the reflections of the $L1_0$ phase with the ⟨100⟩ orientations, Debye-Scherrer rings from the $L1_0$-structure is also seen in the SAED patterns of all specimens, indicating a growth of randomly oriented FePtCu islands together with the ⟨100⟩ oriented growth of FePtCu nanoparticles in the present specimens. The substrate temperature necessary for the perfect epitaxial growth was found to be higher than 613 K in the present sputtering conditions.

Actually, as the substrate temperature increased, the ⟨100⟩ oriented growth was enhanced. In order to know the structural change of FePtCu ternary alloy nanoparticles on substrate heating, diffracted beam intensity profiles measured along [001]* and [110]* directions from the SAED patterns were plotted as a function of reciprocal space distance in Figs. 2(a) and 2(b), respectively. The intensities from 001 and 110 superlattice reflections of the specimen deposited at 563 K are quite weak, and these intensities are largely enhanced at 613 K due to the proceeding of the atomic ordering reaction under the higher substrate temperature. The ordering temperature of 613 K for the $L1_0$-FePtCu nanoparticles is about 260 K lower than that of the $L1_0$-FePt nanoparticles fabricated by our electron-beam deposition.[7,18,19] By contrast, it is clearly shown that the intensity of 111 reflection is largely reduced as the substrate temperature increased, indicating the enhancement of ⟨100⟩ oriented growth under the higher substrate temperature.

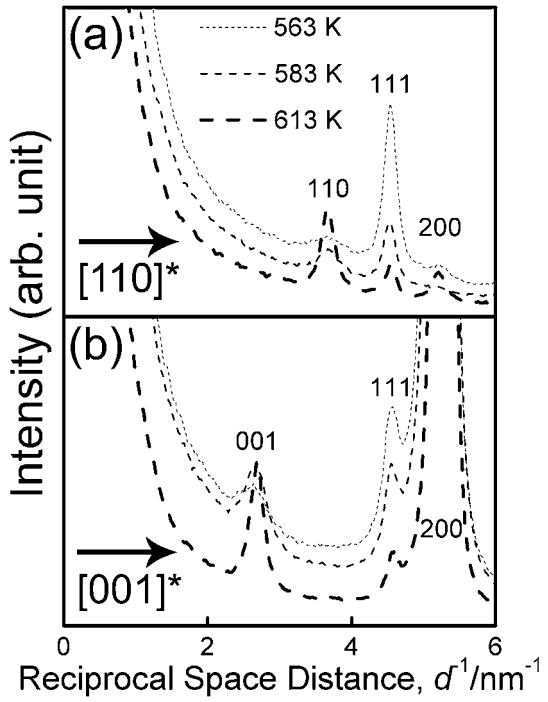

Fig. 2 Substrate temperature dependence of the diffracted beam intensity profiles measured along the (a) [110]* and (b) [001]* direction in the SAED patterns.

Changes of mean particle size, standard deviation and particle areal density against the substrate temperature are

Table 1 Mean particle size (D), standard deviation ($ln\sigma$) and particle areal density (n) for the FePtCu nanoparticles as a function of substrate temperature.

Temperature, T/K	563 K	583 K	613 K
Mean Particle Diameter, D/nm	9.4	9.2	11
Deviation, $ln\sigma$	0.2	0.3	0.23
Areal Density, $n/10^{11}\,cm^{-2}$	7.3	8.0	6.5

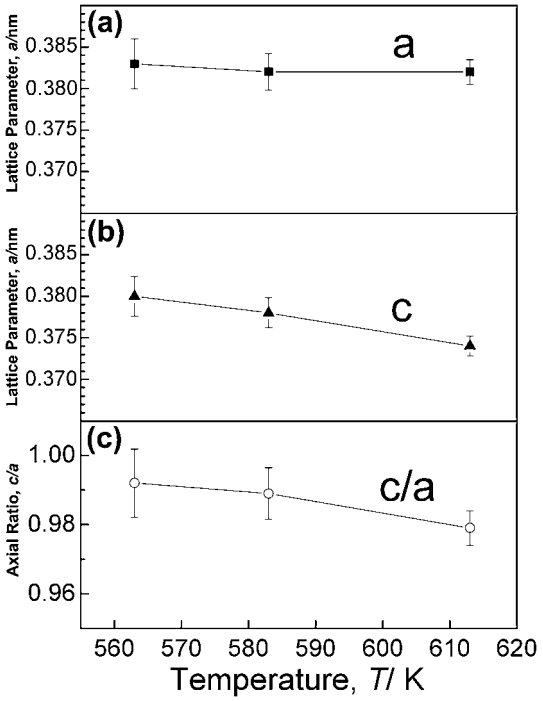

Fig. 3 Lattice parameters of FePtCu ternary nanoparticles as a function of substrate temperature. (a) a-axis, (b) c-axis and (c) axial ratio c/a. The axial ratio c/a is decreased with the increase of substrate temperature due to the evolution of atomic ordering.

listed in Table 1. Particle size is defined as the arithmetical mean of the major and the minor axes of the ellipse.[20,21] The particle sizes followed a log-normal type distribution function which is a characteristic feature frequently observed in deposited metal nanoparticles.[22] Nanoparticles deposited at 613 K have a slightly larger particle size than those of 563 or 583 K due to a larger atom mobility on the substrate surface. Note that all specimens fabricated by the present experiment using rf-magnetron sputtering have the constant particle size deviation ($ln\sigma$) between 0.2 and 0.3 in spite of the variation of mean particle size by the substrate temperature. The particle areal density is in the range of latter half of the $10^{11}\,cm^{-2}$, 1.2–1.6 times lager than that reported previously,[20] and shows no obvious substrate temperature dependence in the temperature range between 563 and 613 K. The areal density largely increased towards $10^{12}\,cm^{-2}$ together with particle size reduction as the sputtering duration decreased.[17]

Lattice parameters of the tetragonal ordered structure, a- and c-axes with axial ratio c/a, are plotted in Fig. 3 against the substrate temperature. Lattice parameters were determined from SAED patterns using a Au fine polycrystalline thin film mounted on a Cu grid as "standard" for the camera-length correction. The a lattice parameter was measured by using the 110 superlattice reflections. In the case of lattice parameter c, 001 superlattice reflections in two kinds of direction were measured and averaged because the FePtCu nanoparticles have two kinds of c-axis direction parallel to the film plane. While the length of a-axis for the $L1_0$-FePtCu nanoparticles did not show a clear substrate temperature dependence, the length of c-axis decreased gradually from 0.380(2) nm to 0.374(1) nm as the substrate temperature increased, resulted in the reduction of axial ratio c/a. Note that the error bar of the lattice parameters denote the standard deviation of the measured lattice parameters. Since the atomic ordering was promoted with the increase of substrate temperature, the degree of atomic order was considered to be very low in the case of specimens deposited at the substrate temperatures of 563 and 583 K. By contrast, the atomic ordering for the specimen deposited at 613 K was much promoted and, simultaneously, the coercivity was also increased with the decrease of axial ratio c/a as shown in the later section 3.2. The measured lattice parameters were $a = 0.382 \pm 0.002$ nm and $c = 0.374 \pm 0.001$ nm with an axial ratio c/a of 0.979 ± 0.005 for the specimen deposited at 613 K with the composition of $Fe_{37}Pt_{51}Cu_{12}$. The obtained axial ratio is slightly larger than those of the well-ordered binary $L1_0$-FePt thin films[23–25] ($c/a = 0.957$ with $S = 0.9 \pm 0.1$,[23] $c/a = 0.964$ with $S = 0.8$[24]) or FePt nanoparticles ($c/a = 0.961$,[19] $c/a = 0.966$[26]). Here S denotes the LRO parameter. Note that a reported axial ratio for a bulk ternary $L1_0$-$FeCuPt_2$ compound is quite low as low as 0.923.[29]

The high-resolution TEM (HREM) micrographs of the FePtCu nanoparticles are shown in Figs. 4(a) (563 K), 4(b) (583 K) and 4(c) (613 K). The characteristic {001} fringes of $L1_0$-ordered phase were observed in the HREM images of all specimens, although these fringes together with 001 superlattice reflection in FFT patterns become obscure as the substrate temperature decreased. Besides the characteristic {001} lattice fringes with lattice spacing of 0.37 nm, also crossed {110} fringes of the $L1_0$-ordered structure with lattice spacing of 0.27 nm are visible in the upper region of the particle in the HREM image for the specimen deposited at 613 K as seen in Fig. 4(c). Note that region with {001} fringes corresponds to the variant with c-axes oriented parallel to the film plane, and that with {110} fringes corresponds to the variant with c-axis oriented perpendicular to the film plane. Hence, the FePtCu nanoparticle shown in Fig. 4(c) consists of two-kinds of crystallographic variants. On the other hand, the {110} lattice fringes are not clearly observed in the HREM images of Figs. 4(a) and (b), although the superlattice reflection of 110 is observed at FFT images weakly. This indicates that the major region in single FePtCu nanoparticle mostly consists of variant-domains with c axis orientation parallel to the in-plane direction. Existence of such a variant-domain structure in a nanoparticle indicates the relatively lower value of degree of order, since the disappearance of the variant domains and the formations of single crystalline nanoparticles with high degree of order were clearly observed on prolonged annealing at 873 K in our previous study on FePt nanoparticles.[19] In the presently

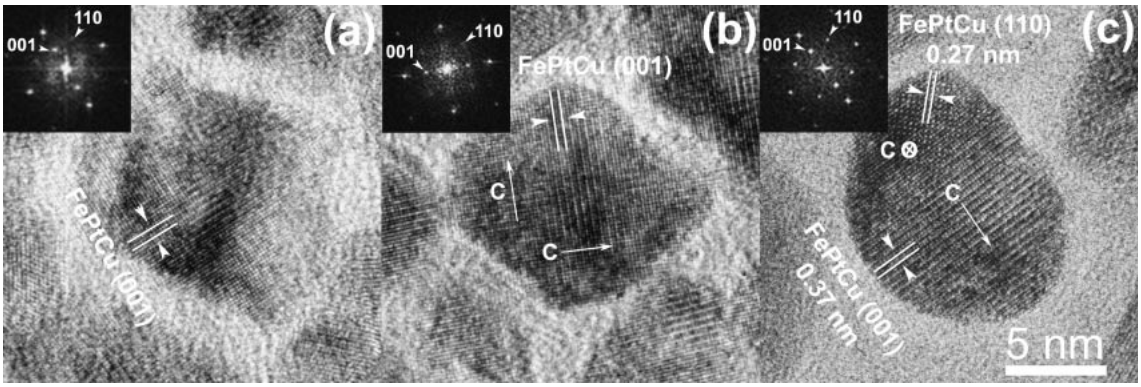

Fig. 4 HREM images of FePtCu nanoparticles formed at (a) 563 K, (b) 583 K and (c) 613 K. {001} lattice fringes are seen in all HREM images but it becomes obscure as the substrate temperature decreased due to the low degree of order. A {110} lattice fringes region is seen in the upper part of the particle in (c), indicating a variant domain formation with *c*-axes normal to the film plane.

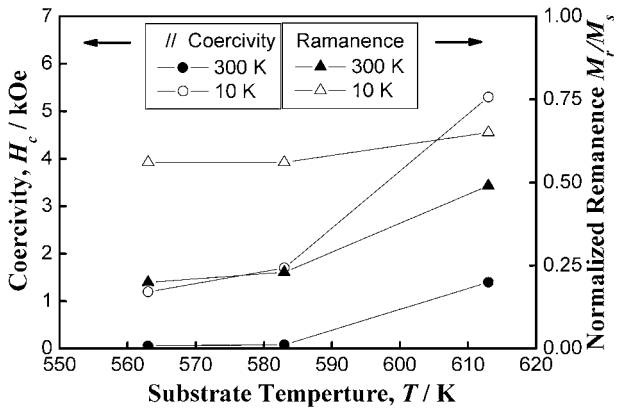

Fig. 5 In-plane coercivities (H_c) and normalized remanence (M_r/M_s) of the FePtCu nanoparticles measured at 10 K and 300 K as a function of substrate temperature. Both the coercivity and the normalized remanence at 300 K are considerably lower than those at 10 K, indicating the existence of thermal fluctuation on magnetization in all specimens.

fabricated FePtCu nanoparticles with the low temperature substrate, the ⟨100⟩ orientational growth of $L1_0$-particles on the NaCl substrate were confirmed.

3.2 Magnetic Property Changes along the Atomic Ordering

Coercivity (H_c) and normalized remanence (M_r/M_s) were obtained from magnetization curves measured with magnetic field along the in-plane direction, and they are plotted against the substrate temperature as shown in Fig. 5. Here, M_r and M_s denote remanence and saturation magnetization, respectively. As the substrate temperature increased, mean particle size increased, hence the horizontal axis of Fig. 5 is related to the particle size. Both coercivity and the normalized remanence at 300 K are considerably lower than those at 10 K, indicating the effect of thermal fluctuation of magnetization in all specimens. It should be noted here that coercivity measured even at 10 K shows particle size dependence as shown in Fig. 5, which can be attributed to the particle size dependence of MAE due to the particle size dependence of LRO parameter. Actually, it has been reported that MAE is proportional to the square of LRO parameter.[27,28] Observed increase of coercivity at 10 K with the increase of substrate temperature indicates the progress of atomic ordering reaction under the higher substrate temperature as revealed by TEM study. The remanences at 10 K show almost constant values around 0.6 in all specimens regardless of the particle size.

Morphologies of the nanoparticles, especially of the crystallographic variants of the $L1_0$-phase, affect the magnetization curves. These are shown in Figs. 6(a) to 6(c) for the specimens synthesized at 563, 583 and 613 K, respectively. The measurements were made at 300 K. The coercivity (1.4 kOe) measured along in-plane direction at 300 K is higher than the coercivity (1 kOe) measured along perpendicular direction as shown in the Fig. 6(c). The higher coercivity for the in-plane direction is well consistent with

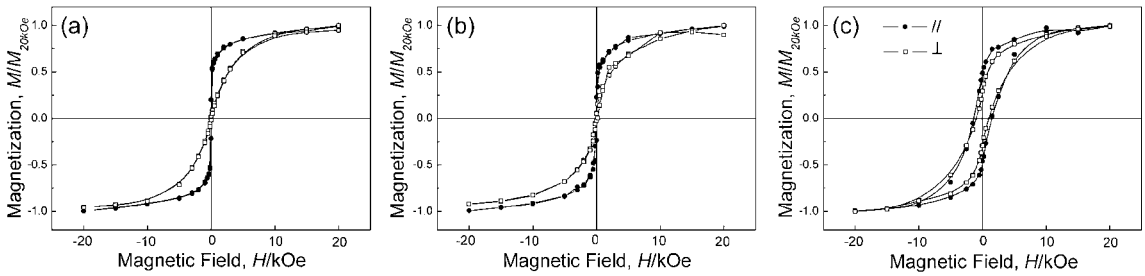

Fig. 6 Coercivities (H_c) of the nanoparticles film formed at (a) 563 K, (b) 583 K and (c) 613 K, which were measured along in-plane (//) and perpendicular direction (⊥) at 300 K.

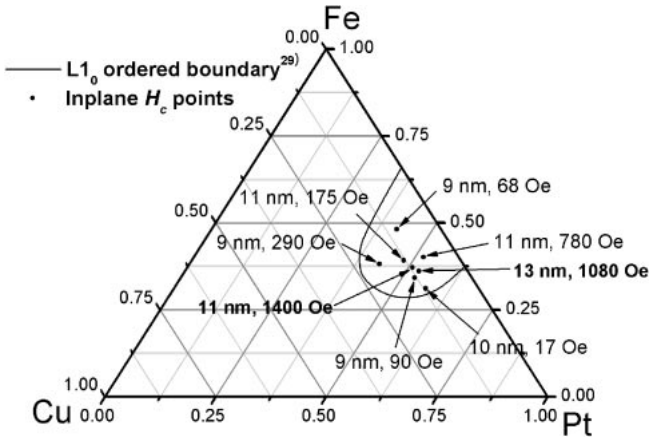

Fig. 7 Composition dependence of the coercivity of the FePtCu ternary nanoparticles sputtered at 613 K. Coercivity sensitively varies depending on the composition of Fe-Pt-Cu. High coercivity more than 1 kOe was obtained at the compositions of Fe-51 at%Pt-12 at%Cu and Fe-53 at%Pt-11 at%Cu.

the result that the major structural region in the FePtCu nanoparticles confirmed by HREM analysis in Fig. 4 consisted of variants with *c*-axes parallel to the film plane. The large change of remanences regarding to the direction of applied magnetic field are seen in Figs. 6(a) and (b). These are also caused by the fact that the variant domains with *c*-axes parallel to the film plane are larger in number than those with *c*-axes perpendicular to the film plane.

Figure 7 shows composition dependence of the coercivity at the substrate temperature of 613 K. In spite of the same sputtering condition except the alloy composition, there observed a tendency that particles with Fe-rich concentration possess relatively smaller particle size. This tendency is presumed to be arose from the morphological change by alloy composition variation. Note that although all specimens were prepared within the solubility limit of the ternary $L1_0$ phase,[29] coercivity showed low values below 0.5 kOe when the Pt composition is less than 50 at% Pt. For example, in spite of almost the same mean particle size around 11 nm in diameter, coercivity of $Fe_{37}Pt_{51}Cu_{12}$ nanoparticles is eight times higher than that of $Fe_{39}Pt_{48}Cu_{13}$ nanoparticles. High coercivity more than 1 kOe was obtained at the compositions of $Fe_{37}Pt_{51}Cu_{12}$ and $Fe_{36}Pt_{53}Cu_{11}$. The coercivity mapping against the alloy composition indicates that the LRO in the FePtCu ternary phase is considered to sensitively depend on the alloy composition. The coercivity change on the alloy composition is through the change of MAE which depends on the composition and LRO of the alloy nanoparticles.

4. Conclusion

$L1_0$-type FePtCu alloy nanoparticles as small as 10 nm with orientation, high-density dispersion and high coercivity have been directly fabricated by co-deposition of Fe, Pt and Cu onto NaCl substrate kept at 563–613 K without any post-deposition annealing using rf-magnetron sputtering. Structure and morphology changes of those particles were investigated by transmission electron microscopy and electron diffraction as a function of the substrate temperature. The $L1_0$-FePtCu ordered phase is formed even at the substrate temperature of 563 K, while the superlattice reflections were quite weak with quite low coercivity. The degree of order drastically enhanced at 613 K resulted in the appearance of clear superlattice reflections and higher coercivity exceeding 1 kOe at room temperature especially when the composition becomes $Fe_{37}Cu_{12}Pt_{51}$. As the substrate temperature increased, ⟨100⟩ oriented growth of FePtCu nanoparticles was enhanced as well as the evolution of atomic ordering. Particle size dependence of LRO is responsible for the decrease of coercivity with particle size reduction as well as thermal fluctuation of magnetization. Coercivity mapping against the alloy composition indicates that the LRO in the FePtCu ternary phase is considered to sensitively depend on the alloy concentration. Alloy composition dependence of MAE and/or LRO parameter is still open questions together with the reason for the achievement of atomic ordering at such a lower temperature as low as 613 K for ternary FePtCu nanoparticles. Studies to know these reason are now underway.

Acknowledgment

This study was partly supported by the Grant-in-Aid for Scientific Research (S) (No. 16106008) from the Ministry of Education, Culture, Sports, Science and Technology, Japan.

REFERENCES

1) I. R. McFadyen, E. E. Fullerton and M. J. Carey: Mater Res Bull **31** (2006) 379–383.
2) O. A. Ivanov, L. V. Solina and V. A. Demshina: Phys. Met. Metallogr. **35** (1973) 81–85.
3) K. Inoue, H. Shima, A. Fujita, K. Ishida, K. Oikawa and K. Fukamichi: Appl. Phys. Lett. **88** (2006) 102503-1–102503-3.
4) D. Weller and A. Moser: IEEE Trans. Magn. **35** (1999) 4423–4439.
5) S. Okamoto, O. Kitakami, N. Kikuchi, T. Miyazaki, Y. Shimada and Y. K. Takahashi: Phys. Rev. B **67** (2003) 094422-1–094422-7.
6) S. Sun, D. Weller and C. Murray: *The Physics of Ultra-High-Density Magnetic Recording*, ed. by M. L. Plumer, J. v. Ek, and D. Weller (Springer, New York, 2001) 249–276.
7) B. Bian, K. Sato, Y. Hirotsu and A. Makino: Appl. Phys. Lett. **75** (1999) 3686–3688.
8) S. Sun, C. B. Murray, D. Weller, L. Folks and A. Moser: Science **287** (2000) 1989–1992.
9) X. Sun, S. Kang, J. W. Harrell, D. E. Nikles, Z. R. Dai, J. Li and Z. L. Wang: J. Appl. Phys. **93** (2003) 7337–7339.
10) Y. Endo, N. Kikuchi, O. Kitakami and Y. Shimada: J. Appl. Phys. **89** (2001) 7065–7067.
11) T. Shima, T. Moriguchi, S. Mitani and K. Takanashi: Appl. Phys. Lett. **80** (2002) 288–290.
12) D. Ravelosona, C. Chappert, V. Mathet and H. Bernas: Appl. Phys. Lett. **76** (2000) 236–238.
13) C. H. Lai, C. H. Yang and C. C. Chiang: Appl. Phys. Lett. **83** (2003) 4550–4552.
14) T. Maeda, T. Kai, A. Kikitsu, T. Nagase and J. Akiyama: Appl. Phys. Lett. **80** (2002) 2147–2149.
15) C. L. Platt, K. W. Wierman, E. B. Svedberg, R. van de Veerdonk, J. K. Howard, A. G. Roy and D. E. Laughlin: J. Appl. Phys. **92** (2002) 6104–6109.
16) Y. K. Takahashi, M. Ohnuma and K. Hono: J. Magn. Magn. Mater. **246** (2002) 259–265.
17) H. W. Ryu, H. Naganuma, K. Sato and Y. Hirotsu: Jpn. J. Appl. Phys. **45** (2006) L608–L610.

18) K. Sato, B. Bian and Y. Hirotsu: J. Appl. Phys. **91** (2002) 8516–8518.
19) K. Sato, B. Bian, T. Hanada and Y. Hirotsu: Scr. Mater. **44** (2001) 1389–1393.
20) K. Sato and Y. Hirotsu: J. Appl. Phys. **93** (2003) 7414–7416.
21) K. Sato and Y. Hirotsu: J. Appl. Phys. **93** (2003) 6291–6298.
22) C. G. Granqvist and R. A. Buhrman: J. Appl. Phys. **47** (1976) 2200–2222.
23) A. Cebollada, D. Weller, J. Sticht, G. R. Harp, R. F. C. Farrow, R. F. Marks, R. Savoy and J. C. Scott: Phys. Rev. B **50** (1994) 3419–3422.
24) M. R. Visokay and R. Sinclair: Appl. Phys. Lett. **66** (1995) 1692–1694.
25) Y. Endo, K. Oikawa, T. Miyazaki, O. Kitakami and Y. Shimada: J. Appl. Phys. **94** (2003) 7222–7226.
26) T. J. Klemmer, N. Shukla, C. Liu, X. W. Wu, E. B. Svedberg, O. Mryasov, R. W. Chantrell, D. Weller, M. Tanase and D. E. Laughlin: Appl. Phys. Lett. **81** (2002) 2220–2222.
27) V. V. Maykov, A. Ye. Yermakov, G. V. Ivanov, V. I. Khrabrov and L. M. Magat: Phys. Met. Metallogr. **67** (1989) 76–81.
28) S. Ostanin, S. S. A. Razee, J. B. Staunton, B. Ginatempo and Ezio Bruno: J. Appl. Phys. **93** (2003) 453–457.
29) M. Shahmiri, S. Murphy and D. J. Vaughan: Mineralogical Magazine **49** (1985) 547–554.